NANO LETTERS

Letter

pubs.acs.org/NanoLett

High-Rotational Symmetry Lattices Fabricated by Moiré Nanolithography

Steven M. Lubin,[†] Wei Zhou,[‡] Alexander J. Hryn,[‡] Mark D. Huntington,[‡] and Teri W. Odom*[,†,‡]

[†]Department of Chemistry and [‡]Department of Materials Science and Engineering, Northwestern University, Evanston, Illinois 60208, United States

Supporting Information

ABSTRACT: This paper describes a new nanofabrication method, moiré nanolithography, that can fabricate subwavelength lattices with high-rotational symmetries. By exposing elastomeric photomasks sequentially at multiple offset angles, we created arrays with rotational symmetries as high as 36-fold, which is three times higher than quasiperiodic lattices (≤12-fold) and six times higher than two-dimensional periodic lattices (≤6-fold). Because these moiré nanopatterns can be generated over wafer-scale areas, they are promising for a range of photonic applications, especially those that require broadband, omnidirectional absorption of visible light.

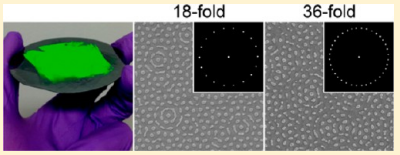

KEYWORDS: *Nanopatterning, quasiperiodic, moiré patterns, high rotational symmetry lattices, soft lithography*

Quasicrystals are ordered materials that do not have translational symmetry but form stable structures with rotational symmetries higher than periodic materials.[1,2] Recently, artificially designed high-symmetry lattices based on quasicrystalline structures have been generated. For example, high-rotational symmetry nanoparticle superlattices with spacings from 4.7 to 13.4 nm have been synthesized,[3] and quasiperiodic dielectric hole arrays with spacings from 180 to 600 nm have been fabricated to control lasing action at visible wavelengths.[4] The design of quasicrystalline arrays with subwavelength spacings is especially important in photonics. Such symmetries can result in full band gaps in photonic crystals,[5−10] transmit electromagnetic waves over a broad spectral range in perforated metallic films,[11−13] and trap light omnidirectionally in patterned photovoltaic devices.[14,15]

The rotational order of an array, n, is the highest positive integer that satisfies a rotation by $360°/n$ that will replicate the pattern. As defined by the crystallographic restriction theorem (CRT), the maximum n-fold rotational symmetry for a periodic lattice in two dimensions is limited to 6-fold (i.e., a hexagonal array).[16] As a result, different spatial arrangements are needed for higher rotational symmetries. Aperiodic patterns with symmetries that exceed the CRT have been investigated for several decades.[17] Quasiperiodic arrays that lack the translational symmetry of periodic arrays but contain 8-fold, 10-fold, or 12-fold rotational symmetries (quasiperiodic symmetries) are the most well-known of these patterns.[18,19]

The fabrication of quasiperiodic lattices at optical wavelengths typically requires direct-write methods because the coordinates of each feature in the array must be individually determined. Electron-beam lithography and focused ion beam milling are the most common serial techniques that can generate substrates with these spacings, but they are slow and can only pattern over limited areas. For example, approximately one week is needed to pattern 160 nm lines spaced 500 nm apart over a 1 cm^2 area with an electron beam operating at 500 kHz and with an exposure dimension of 10 nm.[20] Therefore, parallel nanofabrication techniques that can produce multiple sets of features simultaneously over macroscale areas (>cm^2) would open new opportunities for quasiperiodic lattices. Interference lithography[21] and deep-UV projection mode photolithography[22] have been used to fabricate quasiperiodic masks, which were then used to create three-dimensional (3D) arrays. Although these approaches can pattern large areas, they require experimentally intensive setups. Another strategy to create high-symmetry arrays over macroscale areas exploits the moiré effect, which occurs when periodic layers are superimposed on each other.[10,23,24] This phenomenon is most commonly associated with undesirable effects that arise from the image processing of patterns such as pinstripe or houndstooth.[25] Several applications, however, have taken advantage of the moiré effect for characterization purposes. For example, the absence of a moiré pattern between identical periodic grids etched into a substrate and a photomask indicates good alignment,[26] and the presence of a moiré pattern from the superposition of arrays on secure documents is an efficient anticounterfeiting measure.[27]

Here we report how high-rotational symmetry, subwavelength patterns can be fabricated by moiré nanolithography. We show that multiple UV exposures through transparent, elastomeric masks at different angular offsets can result in superperiodic moiré patterns with subwavelength and microscale feature spacings. At sequential exposure angles of $360°/n$, the overall rotational symmetry of the array could exceed 12-fold, which is the highest rotational symmetry of a 2D quasiperiodic lattice. We determined the design rules for

Received: July 9, 2012
Revised: August 8, 2012
Published: August 16, 2012

   dx.doi.org/10.1021/nl302535p | *Nano Lett.* 2012, 12, 4948−4952

achieving lattices with well-defined rotational symmetries and patterned subwavelength features with rotational symmetries as high as 36-fold. Because moiré nanolithography is a massively parallel method, we can create arrays over macroscale areas where the total patterned area is only limited by the size of the masks.

After a single exposure, phase-shifting photolithography (PSP)[28,29] using composite poly(dimethylsiloxane) (PDMS) masks[30,31] patterned with subwavelength features[32−35] (Figure 1A,B) produces photoresist (PR) patterns that are the same as those on the photomask (Figure 1C,D). Photolithography details can be found in the Supporting Information. To fabricate arrays with rotational symmetries higher than those on the PDMS photomask or allowed by the CRT, we invented a

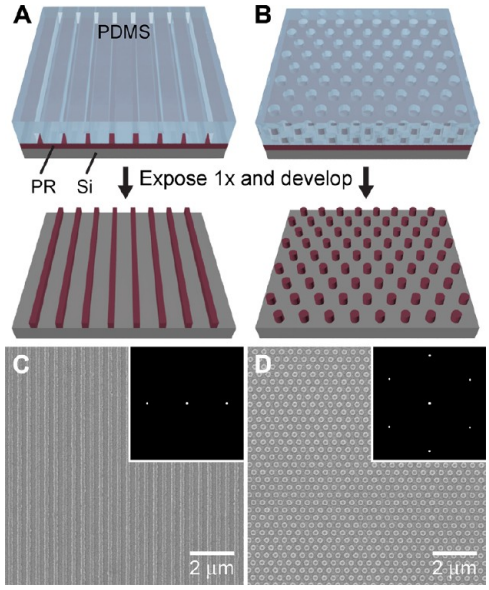

Figure 1. One-to-one patterning of 1D and 2D subwavelength periodic lattices through transparent, PDMS photomasks. Fabrication schemes of (A) linear and (B) hexagonal patterns and (C,D) their SEM images and Fourier transforms (insets).

nanofabrication method called moiré nanolithography. This technique combines the large-area subwavelength patterning capabilities of PSP with the moiré effect by exposing periodically patterned PDMS masks multiples times at an angular offset (α) (Figure 2A). For example, a PDMS mask with an intrinsic rotational order $n' = 6$ (a hexagonal array) exposed twice with the second exposure at $\alpha = 0$, 10, 20, or 30°, produces three types of lattices (Figure 2B−E). Note that for $\alpha = 0°$, the mask was left in contact with the PR layer to eliminate any translational effects. As expected, the resulting pattern was a simple hexagonal array. At $\alpha = 10$ and 20°, superperiodic lattices were fabricated with microscale periodicities proportional to $1/\alpha$ (Supporting Information Figure S1) along with the 400 nm periodicity in the PDMS mask. The rotational order symmetry ($n = 6$) was unchanged at these offset angles. At $\alpha = 30°$, however, the superperiodic lattice became a 12-fold array. This higher rotational symmetry was confirmed by the first-order Bragg peaks in the Fourier transform of the pattern (Figure 2E, inset).

Through moiré nanolithography, lattices with quasiperiodic symmetries can be created from simple 1D and 2D periodic masks. For example, an 8-fold array was fabricated by two

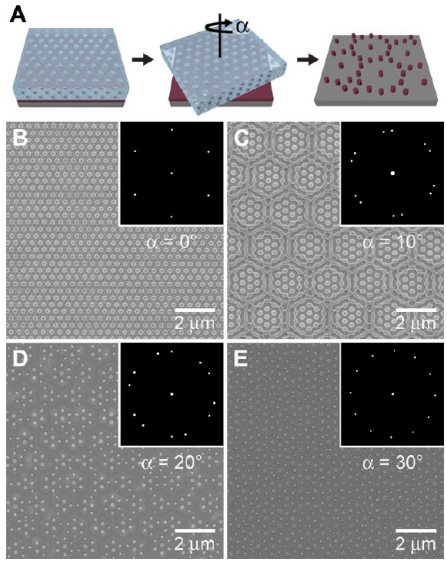

Figure 2. Moiré nanolithography. (A) Fabrication scheme of moiré patterns from a hexagonal PDMS mask exposed twice at an angular offset α. SEM images and (insets) Fourier transforms of the first-order Bragg peaks for (B) a hexagonal array ($\alpha = 0°$), (C) a superperiodic array ($\alpha = 10°$), (D) a superperiodic array ($\alpha = 20°$), and (E) a 12-fold array ($\alpha = 30°$).

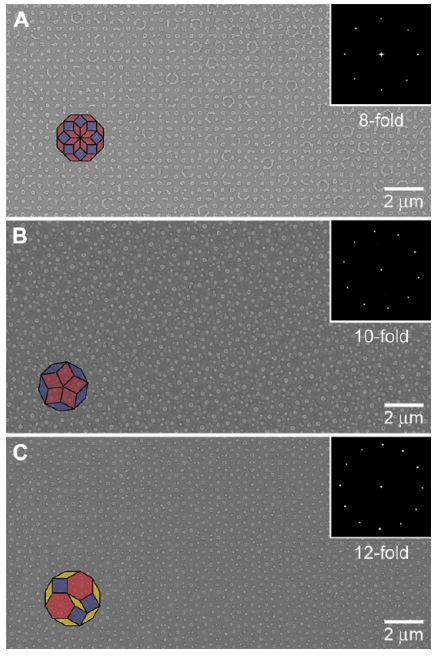

Figure 3. Moiré structures with quasiperiodic symmetries. SEM images and (insets) Fourier transforms of the first-order Bragg peaks of (A) 8-fold, (B) 10-fold, and (C) 12-fold PR-patterned substrates. The shapes on the images represent tiles of 2D quasiperiodic lattices with the same rotational symmetries: Ammann-Beenker tiles for 8-fold, Penrose tiles for 10-fold, and Socolar tiles for 12-fold. The vertices of the tiles are aligned with PR posts generated through moiré nanolithography.

exposures at $\alpha = 45°$ (= 360°/n, where $n = 8$) of a PDMS photomask with a square pattern ($n' = 4$) (Figure 3A). This pattern is similar to Ammann-Beenker tessellations, 8-fold quasiperiodic arrays,[36,37] in that they contain tilings of both squares (blue) and rhombs (45 and 135° interior angles) (red);

dx.doi.org/10.1021/nl302535p | Nano Lett. 2012, 12, 4948−4952

Table 1. Fabrication Conditions for Patterns of Different Rotational Symmetries

	rotational order (n)	base lattice	exposures	angular offset ($\alpha = 360°/n$)
periodic	2	linear ($n' = 2$)	1	none
	4	square ($n' = 4$)	1	none
	6	hexagonal ($n' = 6$)	1	none
quasi	8	square	2	45
	10	linear	5	36
	12	hexagonal	2	30
higher-order	14	linear	7	25.7
	16	square	4	22.5
	18	hexagonal	3	20
	24	hexagonal	4	15
	30	hexagonal	5	12
	36	hexagonal	6	10

however, the moiré pattern does not meet all the requirements for quasiperiodicity in that there is not a complete lack of translational symmetry. A 10-fold pattern can be generated by exposing a PDMS mask with a linear pattern ($n' = 2$) (Figure 1A) five times with $\alpha = 36°$ between each exposure (Figure 3B). Similar to the 8-fold pattern, this moiré array has a quasiperiodic analog in the Penrose lattice.[17] Both patterns contain tessellations of thin rhombs (36 and 144° interior angles) (blue) and thick rhombs (72 and 108° interior angles) (red). Figure 3C shows that a 12-fold array contains tessellations of squares (blue), hexagons (red), and rhombs (30 and 150° interior angles) (yellow) comparable to a Socolar lattice.[38] Although each of these 8-, 10-, and 12-fold patterns was generated through moiré nanolithography, all patterns consist of the same first-order Bragg peaks as their corresponding quasiperiodic lattices.[18,23]

A distinct advantage of moiré nanolithography is that patterned symmetries are not limited to ≤12-fold, the maximum rotational order of 2D quasiperiodic lattices. Since

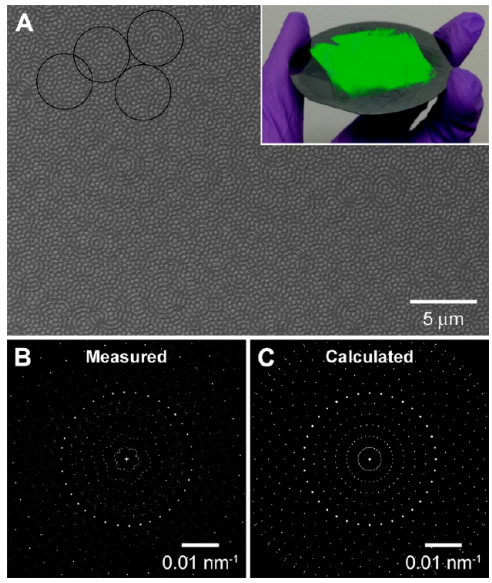

Figure 5. Large-area images of high rotational symmetry moiré patterns and comparison to calculated moiré patterns. (A) SEM image of a 36-fold moiré pattern. The four interlocking circles represent 4 μm rings formed by PR posts. The size of these rings increases with increasing rotational symmetry (inset: photograph of the patterned area on a 3 in. Si wafer.) (B) Fourier transform of the pattern in (A). (C) Calculated Fourier transform of a perfect 36-fold moiré pattern showing the first-order and second-order Bragg peaks.

our nanofabrication method is based on the moiré effect, an unbounded number of patterns can be superimposed to produce lattices with increasingly greater rotational symmetries. We found that three geometric rules govern the fabrication of a desired high-symmetry n-fold lattice. First, n must be an integer multiple of n'. Second, the angular offset between exposures of the PDMS mask must be equal to $360°/n$. Third, the number of exposures at equiangular α must be equal to n/n'. Table 1 outlines parameters from these rules for the fabrication of arrays with rotational symmetries as high as 36-fold, which is

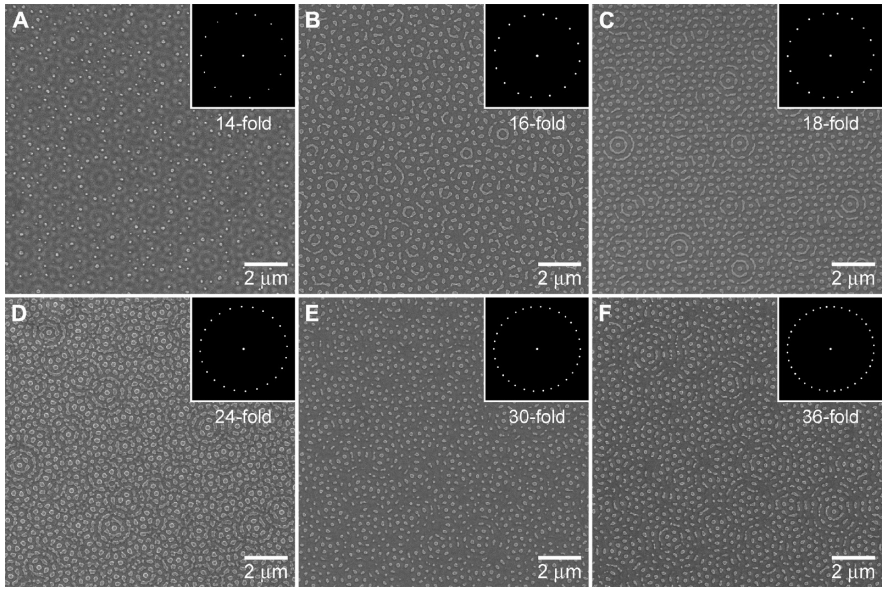

Figure 4. Moiré structures with high-rotational symmetries. SEM images and (insets) Fourier transforms showing the first-order Bragg peaks of (A) 14-fold, (B) 16-fold, (C) 18-fold, (D) 24-fold, (E) 30-fold, and (F) 36-fold PR-patterned substrates.

dx.doi.org/10.1021/nl302535p | Nano Lett. 2012, 12, 4948−4952

three times higher than the highest rotational symmetry order of a quasiperiodic lattice.

Figure 4 displays arrays with rotational symmetries greater than quasiperiodic symmetries from 14-fold to 36-fold. To understand differences in the patterns, where some features seemed to be connected, we created a computational program through MATLAB R2012a (Supporting Information) that simulated the arrays based on three experimental parameters: mask geometry, angular offset (Supporting Information Figure S2), and extent of PR development (Supporting Information Figure S3). Mask geometries were approximated by combinations of 2D sinusoidal waves with periods equal to the periodicity of the arrays (e.g., three in-phase waves with α = 0, 60, and 120° represented a hexagonal mask).[39] A random shift of phase among the sinusoidal waves was also incorporated since translational alignment of PDMS masks with subwavelength features during sequential exposures was not experimentally possible. The PR development extent thus defined a cutoff threshold for the intensity of the wave amplitude. Through this program, we could relate the fabricated arrays with a simulation of their experimental conditions (Supporting Information Figure S4). For example, the PR development for the 24-fold array (Figure 4D) appears to be much less than the other five arrays, and we can simulate how the sample would appear if it were developed more (Supporting Information Figure S5).

Figure 5A highlights the uniformity of high rotational symmetry patterns over a macroscale area (ca. 25 cm^2). A zoomed-in 35 μm × 25 μm region shows that the intricate moiré pattern of a 36-fold array consists of overlapping 4 μm rings composed of 36 PR posts (black circles). The reflected light from the substrate appears green because of the diffraction of visible light from the subwavelength array; the size of the patterned area is limited only by the size of the PDMS mask (Figure 5A, inset). Figure 5B depicts the Fourier transform of the 36-fold array where the brightest ring of spots are from the first-order Bragg peaks, and all other spots away from the center represent higher-order peaks. Figure 5C represents the calculated Fourier transform of a perfect 36-fold moiré pattern. The spots shown are the 36 first-order peaks and the 648 second-order peaks, which are formed by linear combinations of the first-order reciprocal vectors. The first-order peaks from the experimental and calculated Fourier transforms match well with each other; however, the locations of the second-order peaks showed deviations. For example, the five second-order rings with radii less than the first-order ring in the calculated transform consist of 36 evenly spaced peaks, as expected. In the experimental Fourier transform, however, these rings are 6-fold structures. This difference is from misalignments in α during multiple exposure steps, and these inadvertent shifts are highlighted more in second-order peaks.

In conclusion, we have introduced moiré nanolithography as a new technique to generate subwavelength lattices with high rotational symmetry over macroscale areas. Substrates were fabricated with rotational symmetries up to three times higher than quasiperiodic lattices (≤12-fold) and six times higher than 2D periodic lattices (≤6-fold). The substrates can be created with subwavelength spacings over wafer-scale areas, which is favorable for the fabrication of photonic devices to manipulate visible light. We anticipate that these arrays with unique high-rotational symmetries can be useful for the design of new lasing systems, photonic crystals with complete band gaps, and photovoltaic devices with improved light trapping capabilities.

■ ASSOCIATED CONTENT

Ⓢ Supporting Information

Photolithography details, superperiodicity versus angular offset, details of code for calculated Fourier transforms, and computational moiré patterns. This material is available free of charge via the Internet at http://pubs.acs.org.

■ AUTHOR INFORMATION

Corresponding Author

*E-mail: todom@northwestern.edu.

Notes

The authors declare no competing financial interest.

■ ACKNOWLEDGMENTS

S.M.L. was supported by the National Science Foundation (NSF) under NSF Award Numbers DMR-1006380 and DMR-084396. W.Z. was supported by the NSF-MRSEC program at the Materials Research Science and Engineering Center (MRSEC) at Northwestern University under NSF DMR-1121262. A.J.H. was supported by NSF CMMI-1069180 and acknowledges a Hierarchical Materials Cluster Program (HMCP) Fellowship. H.M.C.P. is sponsored by The Graduate School at Northwestern University. M.D.H. was supported by the Department of Defense (DoD) through the National Defense Science and Engineering Graduate Fellowship (NDSEG) Program. M.D.H. gratefully acknowledges support from the Ryan Fellowship and the Northwestern University International Institute for Nanotechnology. This work made use of the NUANCE Center facilities, which are supported by NSF-MRSEC, NSF-NSC, and the Keck Foundation, and the Materials Processing and Microfabrication Facility, which is supported by the MRSEC program of the NSF (DMR-1121262).

■ REFERENCES

(1) Shechtman, D.; Blech, I.; Gratias, D.; Cahn, J. W. *Phys. Rev. Lett.* **1984**, *53*, 1951−1953.
(2) Levine, D.; Steinhardt, P. J. *Phys. Rev. Lett.* **1984**, *53*, 2477−2480.
(3) Talapin, D. V.; Shevchenko, E. V.; Bodnarchuk, M. I.; Ye, X.; Chen, J.; Murray, C. B. *Nature* **2009**, *461*, 964−967.
(4) Notomi, M.; Suzuki, H.; Tamamura, T.; Edagawa, K. *Phys. Rev. Lett.* **2004**, *92*, 123906.
(5) Zoorob, M.; Charlton, M.; Parker, G.; Baumberg, J.; Netti, M. *Nature* **2000**, *404*, 740−743.
(6) Wang, K.; David, S.; Chelnokov, A.; Lourtioz, J. M. *J. Mod. Opt.* **2003**, *50*, 2095−2105.
(7) Kaliteevski, M.; Brand, S.; Abram, R. *J. Phys.: Condens. Matter* **2004**, *16*, 1269−1278.
(8) Parker, G. J.; Charlton, M. D. B.; Zoorob, M. E.; Baumberg, J. J.; Netti, M. C.; Lee, T. *Philos. Trans. R. Soc. London, Ser. A* **2006**, *364*, 189−199.
(9) Florescu, M.; Torquato, S.; Steinhardt, P. J. *Phys. Rev. B* **2009**, *80*, 155112.
(10) Jia, L.; Bita, I.; Thomas, E. L. *Adv. Funct. Mater.* **2012**, *22*, 1150−1157.
(11) Matsui, T.; Agrawal, A.; Nahata, A.; Vardeny, Z. V. *Nature* **2007**, *446*, 517−521.
(12) Agrawal, A.; Matsui, T.; Vardeny, Z. V.; Nahata, A. *Opt. Express* **2008**, *16*, 6267−6273.
(13) Pacifici, D.; Lezec, H. J.; Sweatlock, L. A.; Walters, R. J.; Atwater, H. A. *Opt. Express* **2008**, *16*, 9222−9238.
(14) Huang, Y.-F.; Chattopadhyay, S.; Jen, Y.-J.; Peng, C.-Y.; Liu, T.-A.; Hsu, Y.-K.; Pan, C.-L.; Lo, H.-C.; Hsu, C.-H.; Chang, Y.-H.; Lee, C.-S.; Chen, K.-H.; Chen, L.-C. *Nat. Nanotechnol.* **2007**, *2*, 770−774.

(15) Zhou, W.; Tao, M.; Chen, L.; Yang, H. *J. Appl. Phys.* **2007**, *102*, 103105.
(16) Hiller, H. *Acta Crystallogr., Sect. A* **1985**, *41*, 541−544.
(17) Penrose, R. *Bull. Inst. Math. Appl.* **1974**, *10*, 266−271.
(18) Steinhardt, P. J.; Ostlund, S. *The Physics of Quasicrystals*; World Scientific Pub. Co. Inc.: River Edge, NJ, 1987; p 767.
(19) Janot, C. *Quasicrystals: A Primer*. Clarendon Press; Oxford University Press: Oxford; New York, 1992; p 320.
(20) Altissimo, M. *Biomicrofluidics* **2010**, *4*, 026503.
(21) Bita, I.; Choi, T.; Walsh, M. E.; Smith, H. L.; Thomas, E. L. *Adv. Mater.* **2007**, *19*, 1403−1407.
(22) Shir, D.; Liao, H. W.; Jeon, S.; Xiao, D.; Johnson, H. T.; Bogart, G. R.; Bogart, K. H. A.; Rogers, J. A. *Nano Lett.* **2008**, *8*, 2236−2244.
(23) Amidror, I. *The Theory of the Moiré Phenomenon: Vol. I: Periodic layers*, 2nd ed.; Springer: New York, 2009; p 529.
(24) Balci, S.; Kocabas, A.; Kocabas, C.; Aydinli, A. *Appl. Phys. Lett.* **2011**, *98*, 031101.
(25) Amidror, I.; Hersch, R. *J. Electron. Imaging* **1994**, *3*, 295−317.
(26) King, M. C.; Berry, D. H. *Appl. Opt.* **1972**, *11*, 2455−2459.
(27) Van Renesse, R. L. *Optical Document Security*; Artech House Publishers: London, 2005; p 366.
(28) Rogers, J. A.; Paul, K. E.; Jackman, R. J.; Whitesides, G. M. *Appl. Phys. Lett.* **1997**, *70*, 2658−2660.
(29) Rogers, J. A.; Paul, K. E.; Jackman, R. J.; Whitesides, G. M. *J. Vac. Sci. Technol., B* **1998**, *16*, 59−68.
(30) Odom, T. W.; Thalladi, V. R.; Love, J. C.; Whitesides, G. M. *J. Am. Chem. Soc.* **2002**, *124*, 12112−12113.
(31) Odom, T. W.; Love, J. C.; Wolfe, D. B.; Paul, K. E.; Whitesides, G. M. *Langmuir* **2002**, *18*, 5314−5320.
(32) Henzie, J.; Lee, M. H.; Odom, T. W. *Nat. Nanotechnol.* **2007**, *2*, 549−554.
(33) Henzie, J.; Lee, J.; Lee, M. H.; Hasan, W.; Odom, T. W. *Annu. Rev. Phys. Chem.* **2009**, *60*, 147−165.
(34) Gao, H. W.; Zhou, W.; Odom, T. W. *Adv. Funct. Mater.* **2010**, *20*, 529−539.
(35) Huntington, M. D.; Odom, T. W. *Small* **2011**, *7*, 3144−3147.
(36) Ammann, R.; Grünbaum, B.; Shephard, G. *Discrete Comput. Geom.* **1992**, *8*, 1−25.
(37) Harriss, E. O.; Lamb, J. S. W. *Theor. Comput. Sci.* **2004**, *319*, 241−279.
(38) Socolar, J. E. S. *Phys. Rev. B* **1989**, *39*, 10519−10551.
(39) Toh, K. K. 10th Annual Symposium on Microlithography. *Proc. SPIE* **1991**, *1496*, 27−53.